Comparison of Uncertainty Propagation / Response Surface Techniques for Two Aeroelastic Systems

Matthew S. Allen[1]
University of Wisconsin-Madison, Madison, Wisconsin, 53706, USA

&
José A. Camberos[2]
Air Force Research Laboratory, Dayton, OH 45433, USA

Uncertainty has always been an important consideration when designing, analyzing and testing engineered systems, but computational investigations of the effects of uncertainty are only now beginning to become feasible. Often the limiting factor is the computational expense required to assess the influence of uncertainty on the system. This work provides an overview of techniques that seek to reduce this expense. Sampling methods such as Monte Carlo Simulation (MCS), Latin Hypercube Sampling (LHS) and Low-Discrepancy Sequences will be discussed, as well as reliability methods such as MV, AVM, FORM and SORM. Response surface approximations such as Kriging and Polynomial Chaos will also be discussed, highlighting the fact that all of these uncertainty quantification techniques can be understood in the context of a response surface. The strengths and weaknesses of these uncertainty propagation techniques will be discussed and they will be compared by applying them to two low-order aerospace problems. The examples illustrate a case where most of the methods are not so satisfactory, and another where almost any would perform surprisingly well. Most of these methods are implemented in the Design Analysis Kit for Optimization and Terascale Applications or DAKOTA package, an open source design and optimization toolkit that was created by Sandia National Laboratories beginning in 2001, which was used to perform many of the analyses discussed in the paper.

I. Introduction

ALL systems exhibit some degree of unit-to-unit variability, and even if the system parameters were known perfectly, the methods used to analyze them introduce some level of approximation. For example, the mass and stiffness of aircraft structures can exhibit significant variability, which may cause flutter to occur below the airspeed found by analyzing the nominal structure, or result in limit cycles being observed in regimes other than those predicted by theory. If the system of interest is sensitive to variability, then this can be a critical factor limiting design performance. For example, the mid-frequency acoustic and vibration response of precision space structures is very sensitive to uncertainty, to the point that it may become impossible to make meaningful predictions without considering uncertainty.

One universal challenge in probabilistic design is how to characterize the performance of a system in the presence of uncertainties without incurring astronomical computational cost. This work reviews a number of methods for propagating uncertainty through design models, and shows how all of these methods can be thought of as approximating the relationship between input and output, or the response surface of the system, in some manner. This view is important because it provides considerable insight into the performance of these methods, revealing their relative strengths and limitations. The focus here is on uncertainty quantification in the design stage. A number of methods, including Kriging [2], MARS and various flavors of polynomial chaos [3-5] are applied to two aeroelastic systems, to illustrate these issues. The first consists of a two-degree of freedom airfoil with nonlinear pitch stiffness [6]. The second treats a Goland wing with three wing-stores that have uncertain mass, inertia, positioning and aerodynamic effects. Many of the techniques are implemented using the DAKOTA package [7].

A number of other works have compared uncertainty quantification methods, for example, R. V. Field compared some of the surrogate models considered here in [8]. The work by Giunta et. al [9] is also informative. The purpose of this work is not to provide a detailed review of the voluminous literature on this subject but simply to summarize the features of each method and to explore their strengths and limitations when applied to two aeroelastic systems.

[1] Assistant Professor, Engineering Physics Department, 535 Engineering Research Building, 1500 Engineering Drive, Madison, WI 53706-1609, AIAA Member, msallen@engr.wisc.edu.
[2] Aerospace Engineer, Air Vehicles Directorate, Structures Division, Associate Fellow AIAA.

The following section outlines uncertainty propagation techniques, classifying them as either sampling or response surface techniques and pointing out key differences. While most of what is presented there is available in other publications, those who are not immersed the field will find this section helpful. Section III applies a few representative techniques to a two-degree-of-freedom model of an aeroelastic airfoil and a low-fidelity model of a Goland wing with three uncertain wing-stores. The results are evaluated by visualizing the response surface in each case, which explains why some methods converge slowly or behave erratically. Section IV presents come conclusions.

II. Uncertainty Propagation Techniques

A wide range of uncertainty propagation methods can be classified in two categories: sampling approaches and response surface approaches. The former are commonly used and relatively well understood, so they will be treated only briefly. The focus will be on the latter, especially those which are not always thought of as response surface methods, revealing considerable insight into their performance.

A. Sampling Approaches

Sampling methods, the most well known of which is Monte Carlo Simulation (MCS), simulate what happens when we realize a design. One draws samples at random from each of the random variables or fields comprising the parameters or inputs to a system, and then those values are fed into the analysis model to compute its response. The process is repeated, and one collects statistics on the outputs to quantify, for example, the probability that the response exceeds some threshold. The MCS method is most commonly employed using random sampling (RS), where the samples are generated by a quasi-random number generator on a digital computer. Other possibilities also exist, as discussed subsequently.

The MCS method is versatile, easy to use, and applicable to virtually any uncertainty problem. Its primary drawback is that many samples may be required for some statistics to converge, so the method can be very computationally expensive. For example, if the MCS method is used to estimate the probability that a response metric exceeds some critical level, or the probability of failure p_f, the coefficient of variation (COV) of the estimate is given by the following

$$COV = \sqrt{\frac{\left(1 - p_f\right)}{p_f N}} \tag{1}$$

where N is the number of MCS samples used to estimate p_f. To obtain a small COV, or an estimate with high confidence, one must use a very large number of samples, especially if p_f is low. For example, if p_f =0.0001, one needs almost one million samples to obtain a coefficient of variation less than 10%. On the other hand, other statistics converge much more quickly, such as the mean or standard deviation of the response,.

One important issue when employing a sampling method is the dispersion of the random samples in the parameter space. This is particularly important if very small N is employed, in which case it is likely that the samples obtained will be clustered in the parameter space leaving large regions unsampled. The Latin Hypercube Sampling (LHS) [10, 11] approach seeks to improve on MCS by dividing the parameter space into bins and assuring that exactly one sample is taken from each bin. McKay proved that the LHS estimates have a lower variance than those obtained by random sampling if the system and estimator are monotonic [10], but one cannot necessarily be assured of superior performance in all cases. The advantage of the LHS approach over RS vanishes for larger sample sizes, but there is ample evidence that it does provide better results if the sample size is small.

The random samples generated on digital computers for use in MCS are sometimes called quasi-random numbers because deterministic computers cannot produce a truly random result. Most quasi-random number generators tend to give sample sets that are clustered in the parameter space, so the samples converge very slowly to the desired distributions. Numerous works have presented alternatives that improve the uniformity of the quasi-random samples. Some of the most common alternatives are Hammersley sequences [12], Halton sequences [13] and Latinized Centroidal Voronoi Tessellation (LCVT) [14]. Various works have demonstrated the improved stratification of these methods [4]. For example, consider the two sample sets shown in Figure 1. These were acquired by sampling two uniform random variables with a pseudo-random sampling algorithm [15] and using the Hammersley algorithm [12]. The top panels show that the pseudo-random sampling method clusters some of the samples in the parameter space, while the Hammersley set is evenly distributed over the parameter space. This is

confirmed in the bottom panels, which show histograms of each sample set. The distribution of the sample set obtained by the Hammersley method approximates the true uniform distribution much more closely than that obtained by pseudo-random sampling. On the other hand, the sample set obtained by MCS is certainly plausible, because each sample is random so this sample set could very well have been obtained in a real experiment.

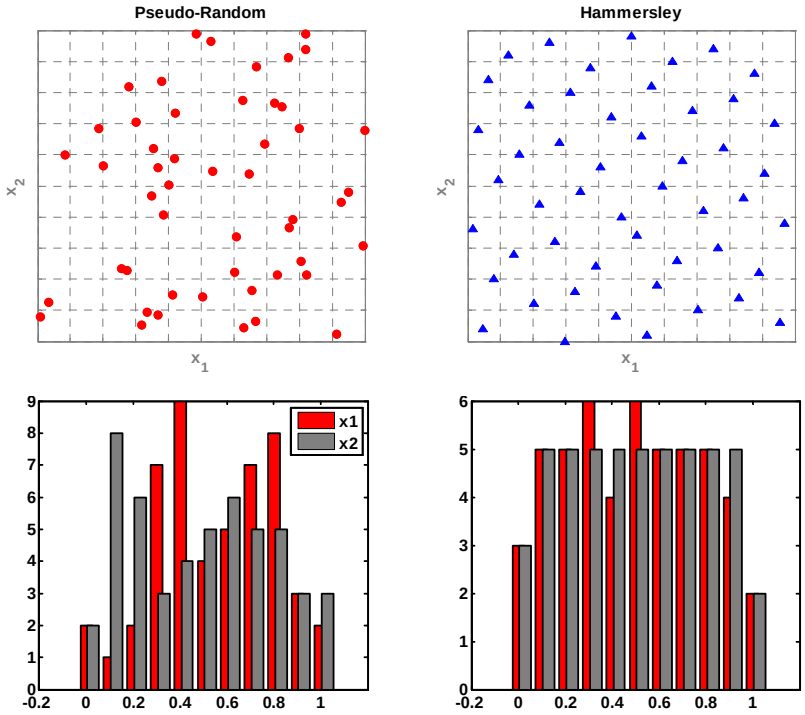

Figure 1: (top) Representative sets of N=50 for two uniform random variables generated using pseudo-random sampling and Hammersley sampling. (bottom) Histograms of each random variable for both sampling methods.

Discussion

Low-dispersion sequences are generally preferred over random sampling, but there are some limitations. For example, section III.A illustrates that the convergence of certain statistics may be misleading. Another significant drawback is that all of these methods produce the entire sample simultaneously, and generally cannot augment a given sample set while maintaining their dispersion characteristics. This is a significant limitation in UQ studies, because one often finds that a particular sample set is too small only after analyzing the statistics, so one would like to be able to increase its size while re-using the samples that were already obtained.

One of the major advantages of the sampling approaches is that they assume virtually nothing about the uncertainty problem; they are universally applicable and one can readily compute the expected variance in the estimates that they provide. This is not necessarily the case for the response surface methods presented in the following subsection.

B. Response Surface Approaches

Response surface methods seek to characterize the relationship between the system's uncertain parameters or inputs and its performance metrics or outputs, or its input-output relationship. In all of the following, let n denote the number of random input variables X in the problem of interest, and m the number of outputs Y of interest. Before delving into the details, it is informative to review a simple example. Figure 2 illustrates a two-dimensional problem. The probability distribution functions of both input variables X_1 and X_2 are shown in red and blue, which define the probability of obtaining any particular combination (X_1, X_2), as illustrated by the contour-plot in the X_1-X_2 plane. Our system is the function relating the inputs to the output, and is shown as a surface that maps the (X_1, X_2) pairs to values of y (third axis). One could find the probability of obtaining a value of y in a particular range by adding up the proportion of the probability in the X_1-X_2 plane that is mapped to that range, and hence create the PDF

of the output *y*. Such an integral is approximated using the MCS method by using a large number of equally probable samples, but a number of other approaches exist. In any event, once the response surface is known, one can completely characterize the uncertain output.

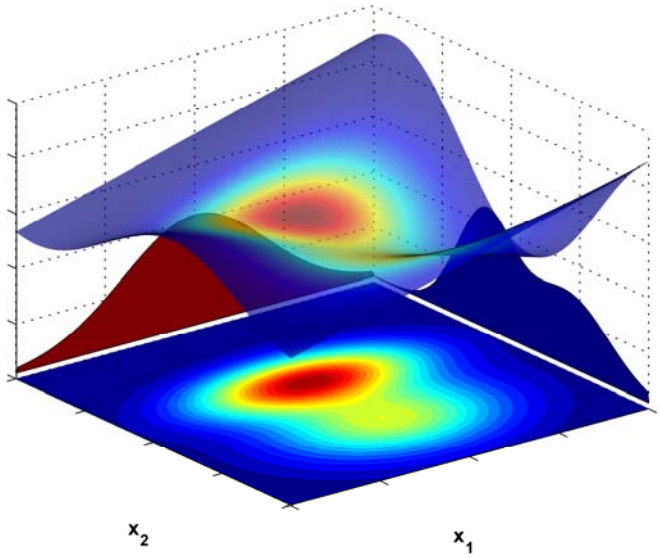

Figure 2: Illustration of 2-dimensional uncertainty propagation. The random variables X_1 and X_2, whose PDFs are illustrated, define the probability of obtaining a sample at each point in X_1-X_2 space. The response surface relates each sample to the output (third axis).

Response surface approximations have the form

$$Y_p = f_p(\mathbf{X}) = \sum_{i=1}^{n_b} c_i h_i(\mathbf{X}) \tag{2}$$

where Y_p is the pth output, $\boldsymbol{X}$ is a vector of random uncertain parameters, $h_i(\mathrm{x})$ is the ith basis function, c_i is its coefficient and n_b the number of basis functions. The approach consists of first selecting a set of basis of functions $h_i(\mathrm{x})$, sampling the output at least n_b times, and then solving a least squares problem with the output and input to estimate the coefficients c_i. One can solve the least squares problem if the basis functions are independent on the space of the sample set. Assuming that the least squares solution is well conditioned, the success of the approach then depends on how well the basis function set $h_i(\mathrm{x})$ approximates the actual surface. Various sets of basis functions have been suggested in the literature, many of which are discussed below.

1. *Polynomial Response Surface*

The formula for a multi-dimensional cubic polynomial response surface is given in [7] as,

$$\hat{f}(\mathbf{x}) \approx c_0 + \sum_{i=1}^{n} c_i x_i + \sum_{i=1}^{n}\sum_{j\geq i}^{n} c_{ij} x_i x_j + \sum_{i=1}^{n}\sum_{j\geq i}^{n}\sum_{k\geq j}^{n} c_{ijk} x_i x_j x_k \tag{3}$$

from which the basis functions can easily be identified. One can obtain a linear or quadratic polynomial by retaining only the first two or first three terms respectively. The number of coefficients to estimate, and hence the number of function evaluations needed to find the surface depends on the order of the polynomial, for example, n+1 evaluations are needed for a first order polynomial, and (n+1)(n+2)/2 for a quadratic surface. Polynomial series are well known, their ability to describe a function (of one variable at least) is well understood, and although they may lead to numerical difficulty at high order, most are aware of this difficulty and many remedies, such as orthogonal polynomials, are available.

2. Polynomial Chaos Expansion (PCE)

From the response surface viewpoint, the Polynomial Chaos Expansion is basically a multi-dimensional polynomial response surface method [5]. This can be seen by noting the basic equation for PCE [7], which can be written as,

$$Y_p = \sum_{i=1}^{n_b} \alpha_i \Psi_i \left(\boldsymbol{\xi} \right) \tag{4}$$

where Y_p is the stochastic response of interest, the basis functions Ψ_i are multi-dimensional orthogonal polynomials of the vector of random variables $\boldsymbol{\xi}$ and α_i are the constant polynomial amplitudes. The random input variables, $\mathbf{X}$, are related to the uncorrelated, standard random variables $\boldsymbol{\xi}$ by some transformation. Various forms of polynomials may be employed, for example, Legendre polynomials are typically employed when the inputs are uniformly distributed. The first few Legendre polynomials are,

$$\Psi_{1,\ldots,4}\left(\xi\right) = \; 1, \quad \xi, \quad 3\xi^2 - 1, \quad 5\xi^3 - 3\xi \tag{5}$$

and it can be shown that the surfaces in equations (3) and (4) can be made to be equivalent for a certain set of coefficient values if $\mathbf{X}=\boldsymbol{\xi}$. If $\mathbf{X}\neq\boldsymbol{\xi}$, then a transformation is employed and the PCE surface, though a polynomial in $\boldsymbol{\xi}$, may not be identical to a polynomial of the same order in $\mathbf{X}$. Orthogonal polynomials also generally lead to better conditioning in the least squares problem used to determine the constants α_i or c_i, but in any event one can think of the PCE as a single-valued, polynomial-like response surface.

3. Kriging and Radial Basis Functions (RBF)

Although the theoretical development of the Kriging approach is somewhat more involved, the response surface concept still applies, where the basis functions decay exponentially with the distance from the training sites [8]. One feature of Kriging models is that they reproduce the values at the training sites exactly; the number of basis functions and associated coefficients is equal to the number training points. One limitation is that the solution for the Kriging surface becomes ill-conditioned as the number of training points increases [7], so there may be an upper limit on the number of training points that can be employed.

4. Multivariate Adaptive Regression Splines (MARS)

The DAKOTA package, which was used in this work, includes the capability to fit a MARS model to a complex response function, as described in [7], and this capability was employed for the Airfoil described in the next section.

5. Relationship to Reliability Methods

Reliability methods can also be viewed in the context of a response surface, although rather than approximating the entire response surface, reliability methods approximate the response surface at a certain response level. In two dimensions, this is the intersection of the response surface with a plane at some value of *Y*, as illustrated in Figure 3, where the intersection or failure surface is represented with a black line. The most probable point (MPP) of failure is also shown. Reliability methods solve an optimization problem to find the MPP, and then approximate the failure surface in some way. For example FORM and SORM [16], approximate the failure surface using linear and quadratic surfaces respectively. A number of researchers are exploring other methods to parameterize the failure surface, such as Kriging-type approximations [17].

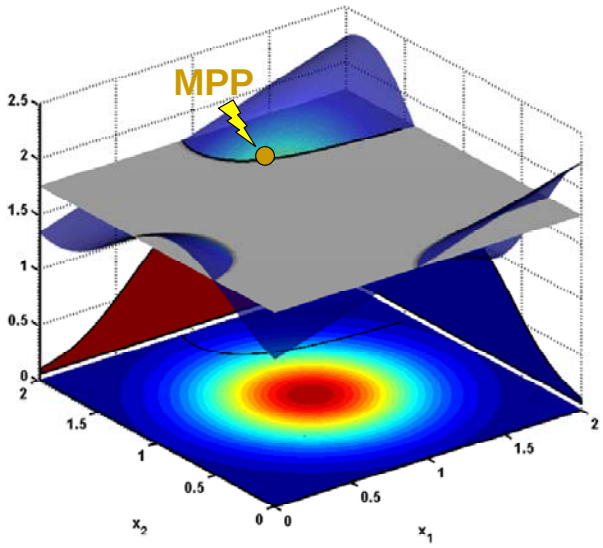

Figure 3: Illustration of Reliability Methods.

The Mean Value (MV) method approximates the response surface using a linear function (a plane in two dimensions) centered at the mean values of each of the random variables using the gradient of the response surface at that point. This method is sometimes restricted to Gaussian input variables, in which case the mean and standard deviations of the output(s) can be readily computed analytically from the gradient and input standard deviations; the output standard deviation only gives a complete description of the output uncertainty if the outputs are all Gaussian. This feature is of little consequence because the method could be readily extended to work with other input distributions. The key to the method is really the linear approximation of the response surface. The mean value second order second moment (MVSOSM) method extends the MV method by approximating the response surface with a multi-dimensional second order polynomial.

A number of variants on the MV method have been proposed. The advanced mean value method (AMV) uses the MV method response surface to find the point in the parameter space at which failure is most likely to occur, and then uses the gradients at that point to approximate the response surface and compute the probability of failure (or, the boundary along which the system just fails, which is the intersection between the response surface and the failure boundary.) AMV+ iterates further until converging on the most probable point of failure. The First Order Reliability Method [16] is also based on a linear approximation of the response surface, but may use a different algorithm to locate the most probable point of failure. These methods have been applied to a variety of systems. See, for example, [18-20].

Reliability methods are sometimes modified by transforming the input variables to standard Gaussian variables (so-called u-space instead of x-space), using, for example, the Rosenblatt transformation [21]. This makes the integrals required to compute the probability of failure simpler, although it may also change the response surface and hence the failure surface. This could be beneficial if it makes the actual input-output relationship more linear, or have the opposite effect if the surface becomes more nonlinear. A response surface that is linear in the space of the original random variables could become nonlinear due to this transformation if the variables are highly non-Gaussian.

One major limitation of these methods is that they require a separate analysis for each output of interest, so they are typically limited to cases where one is only interested in the numerical value of the probability of failure by a single failure mode. In that case, the computational cost required to perform MCS can be tremendous and these methods may achieve the same accuracy with far lower cost. On the other hand, some methods, such as the AMV+ and FORM methods include an iterative solution for the MPP, which may not converge, in which case one might perform thousands of evaluations of the output function and have essentially no useful information at the end. Difficulty with convergence is more likely when the limit state function is nonlinear, and when n is high so that a high order optimization problem must be solved. To the best of the authors' knowledge, none of these methods provide a confidence bound on the estimates of the probability of failure. These methods are implemented in the DAKOTA package, and documented in [7].

III. Examples: Uncertainty Quantification of Two Aeroelastic Systems

A. Nonlinear 2DOF Airfoil of Lee et al. [22]

The first system considered was initially presented by Lee et al. [22], and has been studied by numerous researchers, and examined probabilistically by Millman et al. [6] and Missoum et al. [23]. It consists of a 2DOF airfoil in a flow field, whose aerodynamic effects are modeled using Theodorsen's function [24]. The torsional spring supporting the airfoil has a cubic stiffness component β_α, which may cause the system to exhibit limit cycle oscillation (LCO) near the linear flutter speed if the initial conditions are large enough. As done by Missoum et al. [23], we model the initial pitch angle of the airfoil α_0 as a uniform random variable, with $0 \le \alpha_0 \le 0.6$, as well as the nonlinear stiffness component β_α with $-4.0 \le \beta_\alpha \le 0$. This results in a nonlinear stochastic system with quite a complex response surface, providing a challenging system to test the performance of the UQ methods. The primary objective is to determine the probability that the LCO amplitude exceeds 20 degrees, in which case the system fails to meet its performance requirements, so this is denoted the probability of failure P_f.

In actuality, such a designation is somewhat artificial because there is usually not a precise level at which a system fails; tradeoffs almost always exist in a realistic design problem. Hence, a more useful objective is to determine the probability density function (PDF) or cumulative density function (CDF) of the LCO amplitude, because it tells decision makers how likely a response at any given level is. Because of space limitations, only the probability at 20 and 25 degrees will be reported in the following, but the entire CDF could be estimated using each of the methods below without any additional evaluations of the airfoil model.

Each of the response surface methods described in the previous section was applied to the Airfoil to determine the probability of LCO exceeding 20 and 25 degrees, using the DAKOTA package [7]; the results are shown in Figures 4 and 5 respectively versus the number of training points used to create the response surface. For each method, the probability of failure was predicted using a 10,000 point MCS on the response surface. The PCE method was applied using both N collocation points and $N^{1/2}$ quadrature points per random variable. The implementation in DAKOTA did not allow more than 10 quadrature points per dimension. For the collocation method, the polynomial order was set such that there were twice as many samples as necessary to estimate the PCE coefficients, which was found to be optimal by Hosder [4], so the polynomial orders considered (and associated sample sizes in parenthesis) were 2(12), 3(20), 4(30), 5(42), 6(56), 7(72), 8(90), 9(110), 10(132), and 12(182). The quadrature method used a chaos order of $N^{1/2}$-1.

Kriging was also employed using both Halton and Hammersley [12] sequences of size N = 10, 25 and 50. The Kriging algorithm was attempted for samples sizes of 75 and larger, but DAKOTA's Kriging algorithm failed to converge so the results were not included here. The MARS algorithm was also employed using Hammersley sampling. Two Monte Carlo simulations were also performed. The first used 10,000 samples and is considered the truth model. The probability of failure found by that MCS is shown with a yellow line, as well as the upper and lower 5% confidence bounds on that prediction with dashed lines, so one can ascertain with 90% confidence that the true probability of failure is between the two bounds. The second MCS utilized Hammersley sampling with various values of N, and the probability of failure and 90% confidence interval for that prediction are also shown as a function of N.

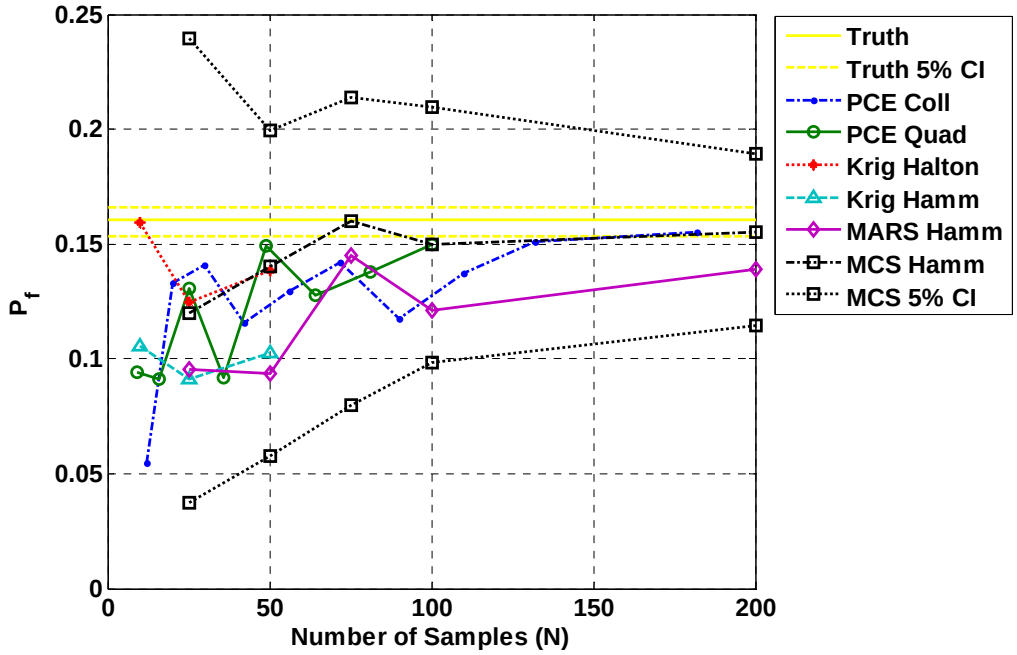

Figure 4: Probability that the LCO amplitude exceeds 20°, estimated using various UQ methods and with various sample sizes.

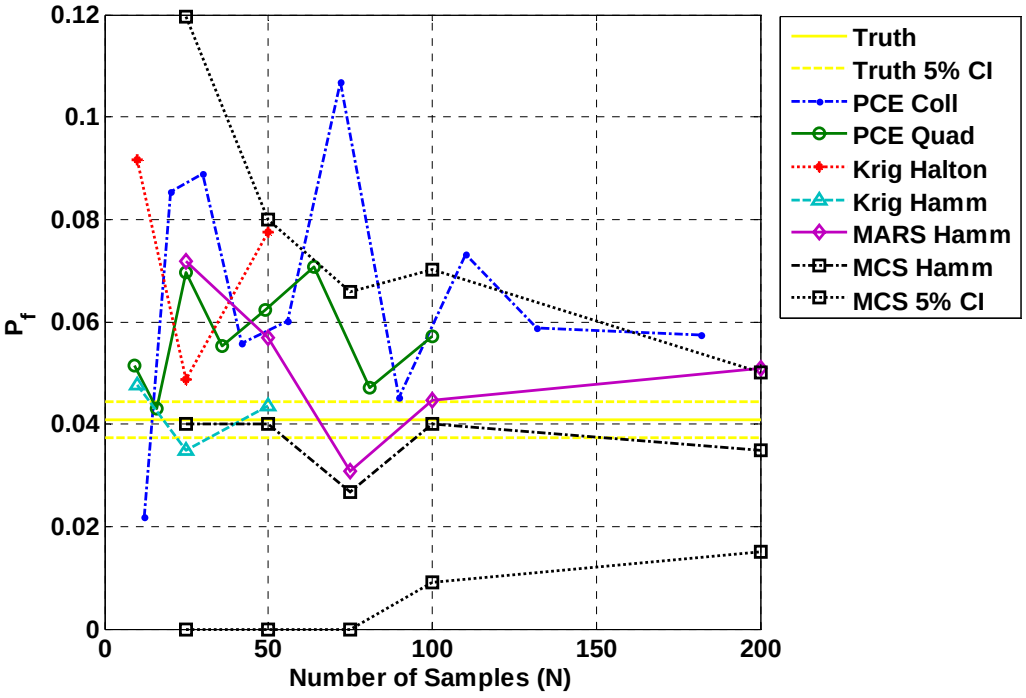

Figure 5: Probability that the LCO amplitude exceeds 25°, estimated using various UQ methods and with various sample sizes.

Figure 4 shows that the collocation PCE method seems to converge for this problem for large enough N, although the convergence is erratic for N<100. At low sample sizes the error in P_f is about 50%, yet within the 90% confidence interval around the MCS result. On the other hand, the collocation PCE method has apparently not yet converged at N = 182 in Figure 5, where the probability of failure is lower, and the convergence is even more erratic. The accuracy of the Kriging surfaces depended strongly on the sampling method; in Figure 4, the surface found with Halton training samples was in error by no more than 25% whereas that found with Hammersley samples was in error by 50% for all three samples sizes. On the other hand, Figure 5 shows the opposite trends for the Kriging method when determining the probability that the response exceeds 25 degrees. The MARS surface has about 50% error at low sample sizes, and that error gradually decreases as the sample size increases.

The probability of failure found using MCS with Hammersley samples is generally more accurate than the predictions found by the other methods for all of these sample sizes, but those methods' predictions are always within the confidence bound on the MCS prediction when the probability of exceeding 20 degrees is relatively large in Figure 4, and usually within the confidence bound in Figure 5 where the probability is smaller.

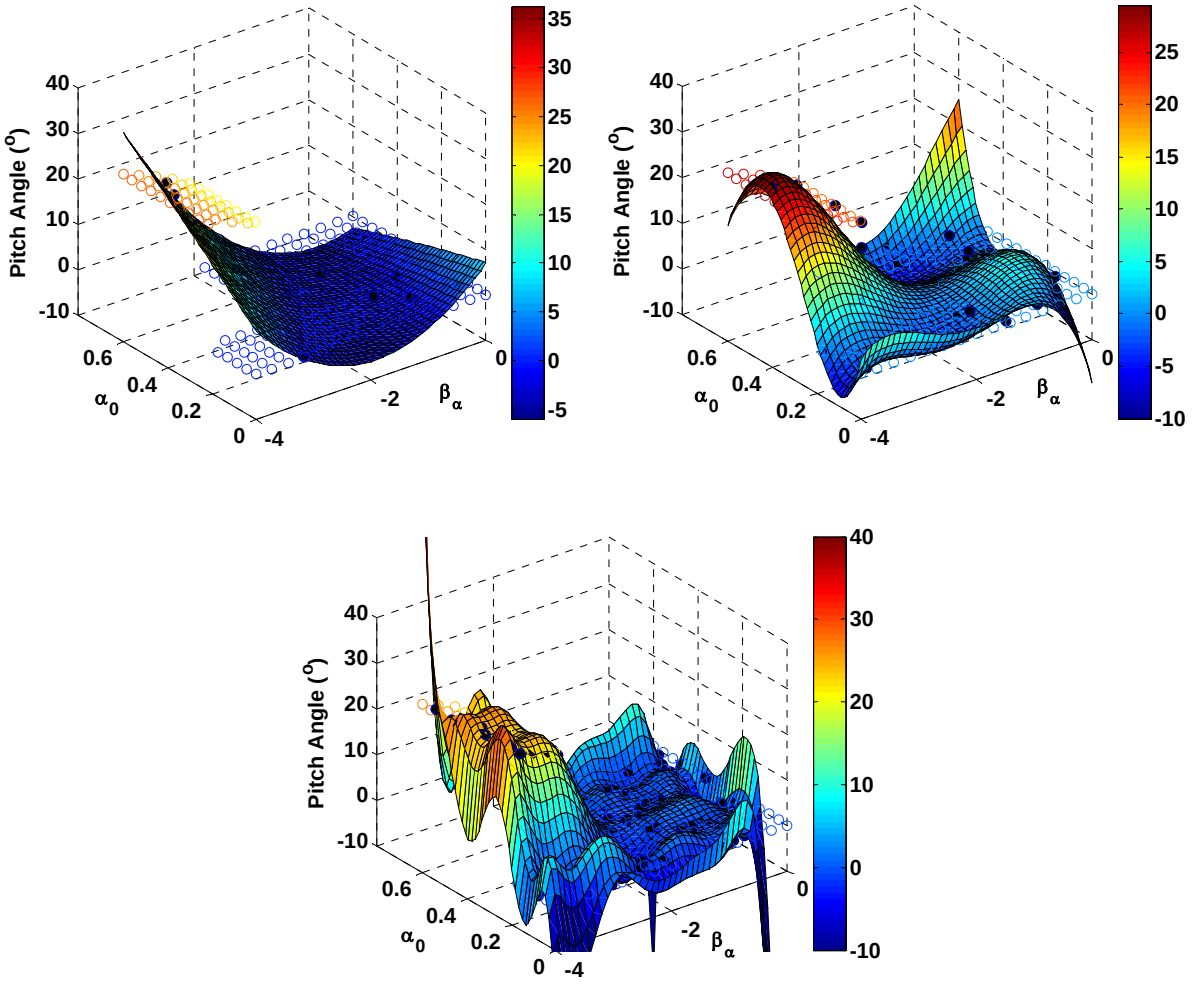

Figure 6: Response surfaces for non-intrusive PCE method for p = 2 (top left), p = 4 (top right) and p = 9 (bottom). Values of the true response surface are shown with colored circles, and the training data are shown with filled black circles.

As discussed previously, each of these methods approximates the response surface. A set of response surfaces obtained with a non-intrusive PCE method [5] for p = 2, 4 and 9, s are shown in Figure 6. Note that we could not determine how to export the response surface found by DAKOTA, so this is not the same PCE algorithm used in Figures 4 and 5 but a separate one written by the authors based on [5]. The values of the true response function,

sampled on a 15 by 15 grid are also show with colored circles, as are the training data with filled black circles, although many of these points are masked by the surface. This figure shows that the PCE polynomial surface converges rather erratically to the true response surface, especially near the edges. The areas in the edges that are most inaccurate correspond to regions in which there was not a training sample (Latin Hypercube Samples were used here [10, 11]); these areas become smaller as the number of samples increases, yet the surface in these areas becomes more erratic as the polynomial order increased. On the other hand, the surface does follow the trend of the data, even at low polynomial orders.

Response surfaces for the Kriging Method at N = 10 and N = 50 are shown in Figure 7, with the same surface displayed both as a 3D surface and a contour plot.

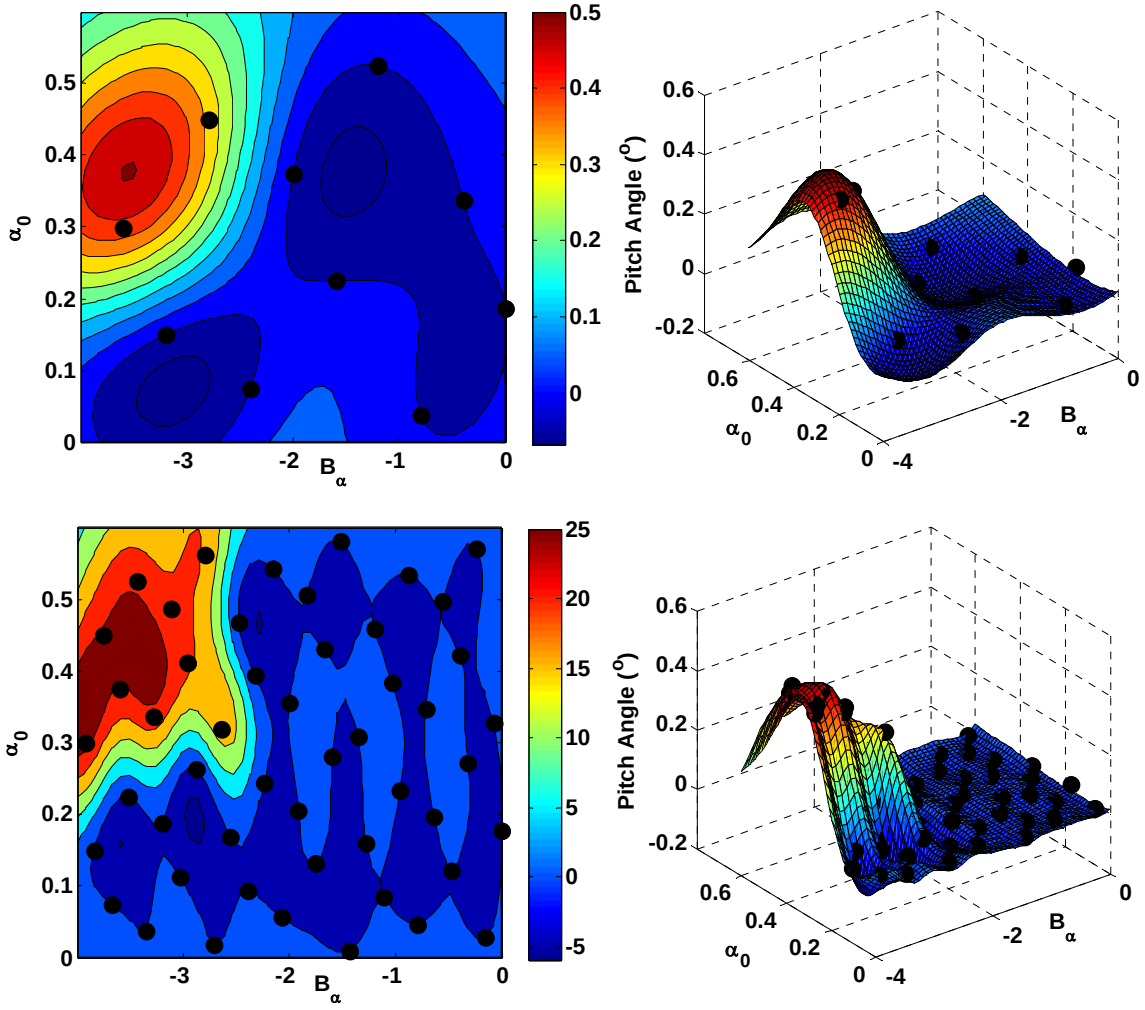

Figure 7: Response surfaces for Kriging method with 10 (top) and 50 (bottom) Hammersley training points. The training data are shown with solid black circles.

The Kriging surface captures the true response surface quite well, even for N = 10, although it is artificially oscillatory at N =50. The Hammersley training samples do not contain a point in the upper left corner for either N = 10 or N = 50, and hence the response surface falls to a low value in that corner. The Halton training samples (not shown) consistently included a sample in the upper left corner, and hence that surface reproduced the actual response surface more accurately.

The response surface obtained by MARS using 200 Hammersley training points is shown in Figure 8. The surface follows the training points closely, except near the discontinuity, where a Gibbs type phenomenon is observed.

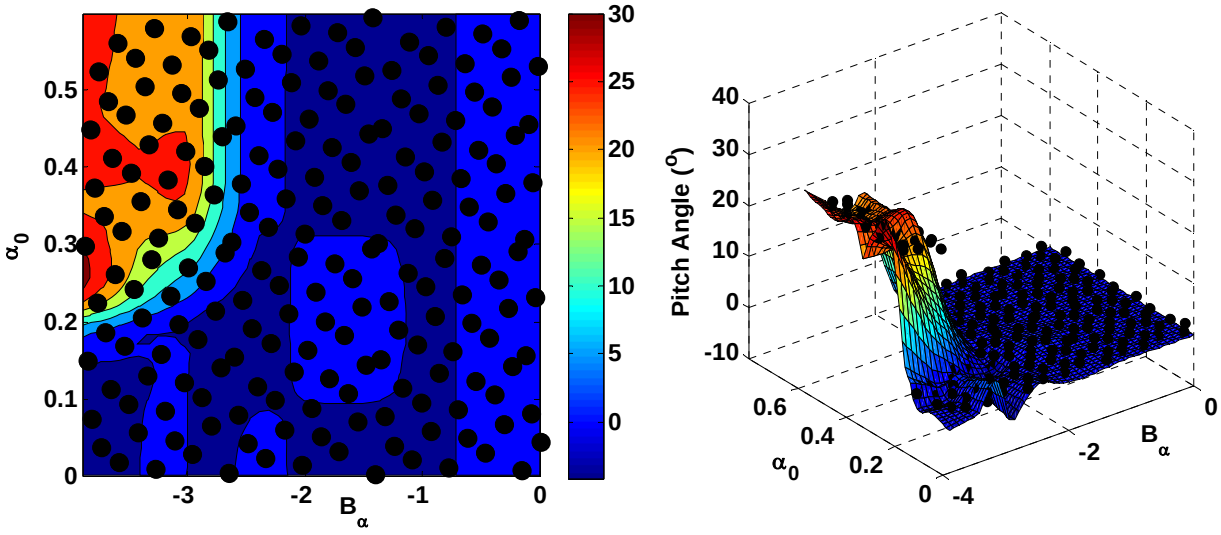

Figure 8: Respnose surface obtained using MARS algorithm with 200 Hammersley training samples. The training data are shown with solid black circles.

Discussion

A number of comments are in order regarding these results. First, it was noted that the PCE converged erratically near the edges of the domain; the value at β_0 = -4 and α_0=0.6 oscillated between many percent too low to many percent too high as the polynomial chaos order increased. When the maximum allowable LCO amplitude was 20 degrees, the failure region was a large portion of the β_0-α_0 plane, so this had only a moderate effect on the convergence. As the size of the failure region decreased, Figure 5 showed that the convergence became more erratic due to this effect.

It was also observed that the Kriging surface obtained with Halton training samples estimated the probability of failure much more accurately than the Kriging surface that used Hammersley training samples. Investigation of the response surfaces suggests that the reason for this is that the Halton scheme placed a sample near the extreme, β_0=-4 and α_0=0.6, edge of the parameter space, while the Hammersley scheme consistently missed that point. This should not be interpreted as an advantage of one scheme over the other; one does not know a priori what region of the parameter space is most critical a priori! On the other hand, this highlights the difficulty of describing a complex, nonlinear response surface with a small number of samples when little is known about its shape a priori.

B. Goland Wing with Uncertain Stores

The second system considered consists of a Goland wing with three wing stores, located at the half, three-quarters and full span of the wing. Figure 9 shows a schematic of the wing with one illustrative store at the wing tip. A similar system was studied by Beran *et. al* in [25].

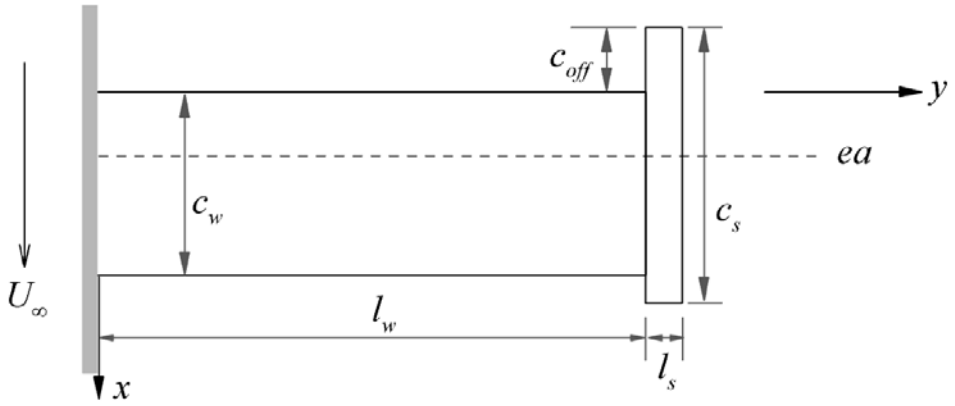

Figure 9: Schematic of Goland wing with a single store at y = (l_w+0.5l_s). (Three stores were employed in the example considered here.)

The frequency domain equations of motion for the Goland wing were found by modifying the example in [24] to include the three stores, and are given in the appendix. The parameters used are given in Table 1. Each of the stochastic parameters is uniformly distributed on the interval given. There are six independent stochastic parameters for each of the three stores, so there are a total of eighteen uncertain parameters.

Deterministic Parameters			**Stochastic Parameters**		
	Value	**Description**		**Range**	**Description**
l_w	20	wing length (ft)	c_s	10 ±25%	store length in chordwise direction (ft)
c	6	wing chord (ft)	a_s	[-0.2, 0.2]b	store attachment point
b	c/2	wing semichord (ft)	y_s	10±5%, 15±5%, [19,20]	spanwise location of store (ft)
a	-0.34	wing elastic axis location (), $a*b$ = distance from wing centerline to elastic axis (ft)	m_s	0.746 ±25%	store mass (slugs)
m	0.746	wing mass per unit length (slugs/ft)	d	[-0.2, 0.2]b	store CG Location (ft) relative to elastic axis
Sy	0.447	wing static imbalance per unit length (slugs-ft/ft)	I_s	2.2 ±25%	store inertia (slugs-ft^2)
Iy	1.943	wing inertia about elastic axis per unit length (slugs-ft^2/ft)			
E	1.4976e9	wing modulus of elasticity (lb/ft^2)	b_s	c_s/2	store semichord (ft) (computed from c_s above)
G	5.616e8	wing shear modulus (lb/ft^2)			
Iea	1.58e-2	area moment of inertia of wing in bending (ft^4)			
J	4.25e-3	area moment of inertia of wing in torsion (ft^2)			
l_s	1.0	store width (ft) in spanwise direction			
ρ_∞	0.002378	air density at sea level (slugs/ft^3)			

Table 1: Parameters of Goland wing model with uncertain stores

The frequency domain equations of motion are given in the appendix and have the form

$$\left[\left[K\right]-\omega^2\left[M+Q\right]\right]\{q\}=0\,. \tag{6}$$

These were solved using the v-g method [24] to obtain the flutter speed of the system. Figure 10 shows a v-g diagram for the system when the store parameters are at their nominal values. The blue and green lines correspond to the frequencies and damping values of the bending and torsional modes respectively. The flutter point is indicated with a red star, and corresponds to a speed of about 300 ft/s. The v-g diagram shows that the flutter speed is a complicated function of air speed; the equations relating the uncertain parameters to the flutter point of the wing are complicated and nonlinear, so it would appear that it might be difficult to describe the flutter speed with a response surface.

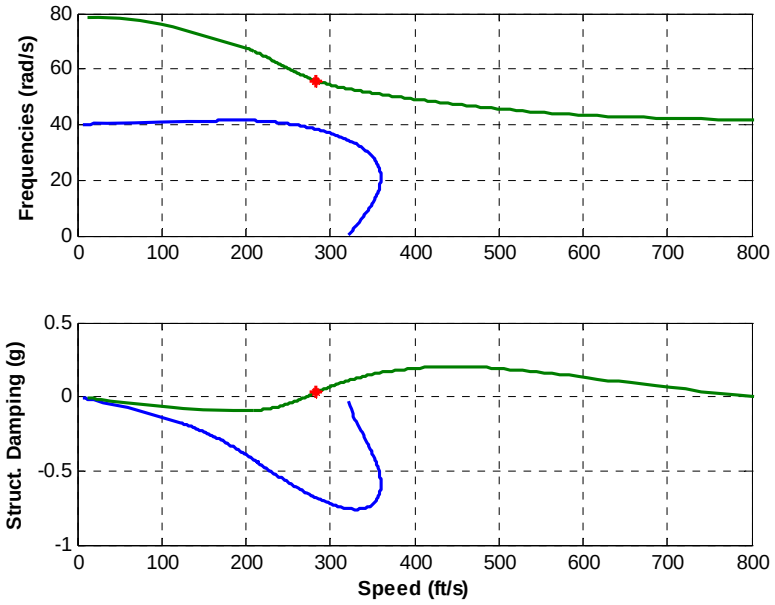

Figure 10: v-g diagram for Goland wing with nominal store parameters.

In order to evaluate the nonlinearity of the response over the range of the uncertain parameters, the model was evaluated with each parameter at its nominal value except one, which was varied over its range. This was repeated for each random parameter. A spider plot was then created showing how the flutter speed depends on each of these parameters, and is shown in Figure 11, revealing that the flutter speed varies as much as 60 ft/s due to a single parameter. The most sensitive parameters are associated with the aerodynamics of the stores, their effective lengths c_s and their attachment points a_s. The flutter speed is approximately linear with respect to these parameters, although some deviation from linearity is observed, especially for c_2 and c_3, which correspond to the lengths of the stores that are at the ¾ span and the tip respectively. (Note that the simplistic methodology used here does not allow one to discover interaction between the parameters. More rigorous approaches are available as described in most texts on Design and Analysis of Computer Experiments (DACE).)

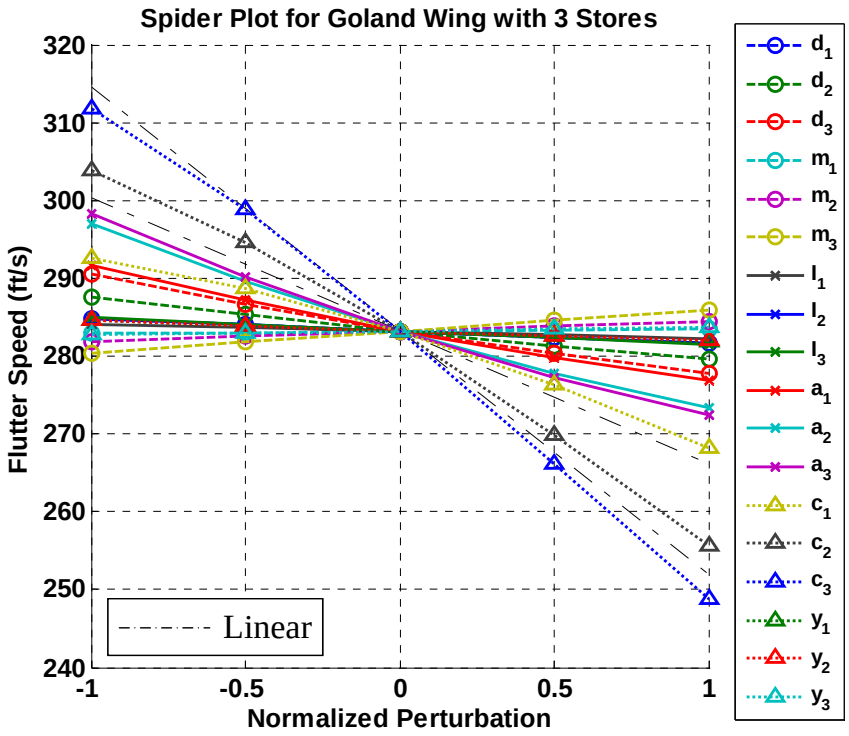

Figure 11: Spider plot showing variation in flutter speed when each of the wing's random parameters is varied independently.

In order to explore the error incurred by using a quasi-linear response surface to describe this system, the PDF of the flutter speed was computed using a simple linear model based on the data in Figure 11 at both extremes of the parameter ranges and at the nominal value. The following response surface was employed for the flutter speed U_f., where $\bar{U}_f$ denotes the flutter speed when the parameters are at their nominal values, $\bar{\theta}_j$ denotes the nominal jth parameter, and θ_j denotes the jth parameter. The upper and lower bounds on each parameter, are denoted θ_j^u and θ_j^l respectively. This surface simply interpolates on Figure 11 for each of the input parameters. A total of 37 evaluations of the simulation code were required to create this surface.

$$U_f = \bar{U}_f + \sum_{k=1}^{18} c_j \left(\theta_j - \bar{\theta}_j\right)$$

$$c_j = \begin{cases} \dfrac{U_f\left(\theta_j^u\right) - \bar{U}_f}{\theta_j^u - \bar{\theta}_j} & \theta_j \geq \bar{\theta}_j \\ \dfrac{U_f\left(\theta_j^l\right) - \bar{U}_f}{\theta_j^l - \bar{\theta}_j} & \theta_j < \bar{\theta}_j \end{cases}. \tag{7}$$

Figure 12 shows the probability density function of the flutter speed calculated in a few different ways. First, 1000 Latin Hypercube samples were used to perform a MCS, and a kernel density estimator [26] was then used to estimate the PDF from the flutter speeds obtained in these 1000 trials. The resulting PDF is considered the truth model and is shown shaded in blue. An MCS was also performed on the response surface described above, and the estimated PDF is shown shaded green. That result agrees quite well with the 1000 sample MCS, suggesting that the simple response surface model is a good approximation for this system; more than 900 additional samples were required to estimate the MCS truth model, so the response surface was much more efficient for this problem.

The response surface prediction was also compared with that of a MCS of similar size, 1,000 randomly selected subsets of size 37, taken from the 1000 sample LHS-MCS, were evaluated. Each of these represents a plausible 37 sample MCS result, and the collection is used to estimate the 95% confidence interval on a 37 sample MCS. The upper and lower confidence bounds are shown with dashed red lines. A representative PDF estimate from a size 37 MCS is shown with a solid red line. There is considerable uncertainty in the PDF estimate based on 37 Monte Carlo samples, so one could obtain a PDF that is considerably different from the true one using that technique.

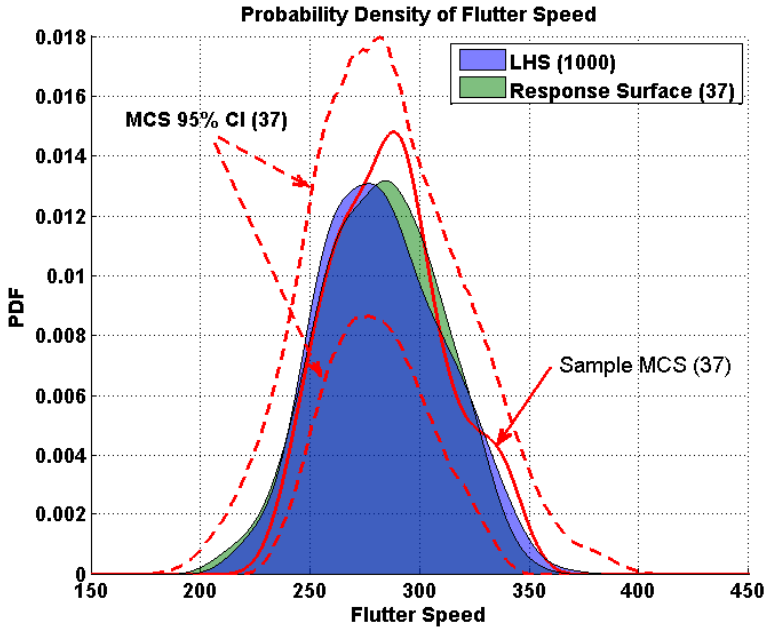

Figure 12: Probability density function (PDF) of flutter speed estimated using three different methods.

Discussion

Although the equations governing this problem are certainly nonlinear, the flutter speed happens to be quite linear over the range of the uncertain parameters. As a result, a low order response surface captures the input-output relationship quite well, and one can obtain a fairly accurate estimate of the output statistics using this response surface. The response surface used here required 2*N+1=37 evaluations of the system model. With such a large number of input uncertainties, the computational cost would quickly escalate if the input-output relationship were even slightly nonlinear, yet this number of uncertainties is common, and perhaps even small for many problems of interest. It is also important to note that while this system was linear in the flutter speed, it is not linear in other outputs of interest, and a poor choice of output parameters may have resulted in a nonlinear response surface.

In this example, we have focused on capturing the general character of the output uncertainties, rather than, for example, the precise probability of failure by some mode. It would also be interesting to focus on the tails of the distributions and see how the methods compare, but such a comparison is only meaningful if the analysis model is thought to be accurate enough to predict the tails, or in other words to predict events that have a very small probability of occurring. For design studies this is often not the case so one must make due with a knowledge of the general character of the uncertainty. One can still profit from knowing, for example, whether the output distribution is unimodal or multi-modal, or what the approximate spread in the output is, or which uncertainties are most important to the output.

IV. Conclusion

Most existing uncertainty quantification techniques seek to approximate the relationship between the uncertain input parameters and the outputs of interest using some pre-defined functional form. This work applied a number of methods to two aeroelastic systems, illustrating that the performance of the methods could be ascertained by considering how well the true response surface is approximated. The first example explored the ability of the response surface methods to capture a highly nonlinear response surface. While the methods quickly captured the

basic essence of the response surface, a large number of training points was required to accurately describe it in detail so that the probability of the LCO amplitude exceeding a certain range could be predicted. The PCE method captured the response surface and converged to the true probability of failure with fewer than 200 samples for this two-parameter problem, yet the convergence was erratic for low polynomial orders, or low numbers of training samples, and was erratic for all polynomial orders at the extreme edges of the parameter space. Also, an anomaly was observed where the Kriging surface greatly underpredicted the probability of failure when Hammersley sampling was used, because that sampling method did not happen to include a sample in a specific region in the parameter space that happened to be critical.

The second example comprised a system which, based on the observations in the first problem, one might expect to be difficult to tackle using a response surface because there were many uncertain parameters and because its overall behavior was highly nonlinear. Surprisingly, the analysis revealed that the system was well approximated as linear over the range of the uncertain parameters, so even a rudimentary response surface was quite effective. This example illustrates that response surface techniques such as these can result in substantial computational savings in cases where one might expect otherwise.

The most important conclusion that this work has elucidated is that there is great utility in considering the response surface employed by the various uncertainty quantification techniques; the critical factor that determines whether these response surface methods succeed or fail is how well they are capable of reconstructing the true system's response surface from a small number of samples. This knowledge can be used to understand when each method is most suitable, and to identify potential pitfalls in a given analysis.

Appendix

The aerodynamics of the wing were modeled using strip theory and Theodorsen's function, as derived in [24] for a 2DOF wing without stores (result found in equations (9-89) and (9-90)). Using the kinetic and potential energy expressions given in [24], we obtain the following expressions for the *j-n*th elements of the mass *M* and stiffness *K* matrices of the wing, and for the dynamic effect of the aeroelastic forces *Q*.

$$M_{jn} = \begin{cases} \int_0^1 m(y) f_{w_j}(y) f_{w_n}(y) dy + \sum_{s=1}^{Ns} (m_s / l_w) f_{w_j}(y_s) f_{w_n}(y_s) & \begin{matrix} j=1...N_w \\ n=1...N_w \end{matrix} \\ -\int_0^1 S_y(y) f_{w_j}(y) f_{\theta_n}(y) dy + \sum_{s=1}^{Ns} (S_s / l_w) f_{w_j}(y_s) f_{\theta_n}(y_s) & \begin{matrix} j=1...N_w \\ n=N_w+(1...N_\theta) \end{matrix} \\ \int_0^1 I_y(y) f_{\theta_j}(y) f_{\theta_n}(y) dy + \sum_{s=1}^{Ns} (I_s / l_w) f_{\theta_j}(y_s) f_{\theta_n}(y_s) & \begin{matrix} j=N_w+(1...N_\theta) \\ n=N_w+(1...N_\theta) \end{matrix} \end{cases} \tag{8}$$

$$K_{jn} = \begin{cases} \int_0^1 \frac{EI}{l_w^4} f''_{w_j}(y) f''_{w_n}(y) dy & \begin{matrix} j=1...N_w \\ n=1...N_w \end{matrix} \\ \int_0^1 \frac{GJ}{l_w^2} f'_{\theta_j}(y) f'_{\theta_n}(y) dy & \begin{matrix} j=N_w+(1...N_\theta) \\ n=N_w+(1...N_\theta) \end{matrix} \end{cases} \tag{9}$$

$$
Q_{jn} = \pi\rho_\infty \begin{cases}
L_h \int_0^1 b^2 f_{w_j}(y)\, f_{w_n}(y)\, dy + \sum_{s=1}^{Ns} b_s^{\,2} (l_s / l_w) L_h f_{w_j}(y_s)\, f_{w_n}(y_s) & \begin{matrix} j=1\ldots N_w \\ n=1\ldots N_w \end{matrix} \\
-\left(L_\alpha - L_h(a+0.5)\right) \int_0^1 b^3 f_{w_j}(y)\, f_{\theta_n}(y)\, dy + & \\
\quad -\sum_{s=1}^{Ns} b_s^{\,3} (l_s / l_w)\left(L_\alpha - L_h(a_s+0.5)\right) f_{w_j}(y_s)\, f_{\theta_n}(y_s) & \begin{matrix} j=1\ldots N_w \\ n=N_w+(1\ldots N_\theta) \end{matrix} \\
-\left(M_h - L_h(a+0.5)\right) \int_0^1 b^3 f_{\theta_j}(y)\, f_{w_n}(y)\, dy + & \\
\quad -\sum_{s=1}^{Ns} b_s^{\,3} (l_s / l_w)\left(M_h - L_h(a_s+0.5)\right) f_{\theta_j}(y_s)\, f_{w_n}(y_s) & \begin{matrix} j=N_w+(1\ldots N_\theta) \\ n=1\ldots N_w \end{matrix} \\
\left(M_\alpha - (M_h + L_\alpha)(a+0.5) + L_h(a+0.5)^2\right) \int_0^1 b^4 f_{\theta_j}(y)\, f_{\theta_n}(y)\, dy + & \\
\quad \sum_{s=1}^{Ns} b_s^{\,4} (l_s / l_w)\left(M_\alpha - (M_h + L_\alpha)(a_s+0.5) + L_h(a_s+0.5)^2\right) f_{\theta_j}(y_s)\, f_{\theta_n}(y_s) & \begin{matrix} j=N_w+(1\ldots N_\theta) \\ n=N_w+(1\ldots N_\theta) \end{matrix}
\end{cases} \tag{10}
$$

where y is the nondimensional position along the span of the wing such that yl_w is the position in feet, and the other parameters are given in Table 1. N_s is the number of stores attached to the wing, N_w the number of bending modes, and N_θ the number of torsional modes used in the Ritz description. These parameters are respectively 3, 1 and 1 in the example used in this paper. The aerodynamic forces are functions of the reduced frequency k and are given by

$$L_\alpha = 0.5 - i(1/k)\left(1 + 2C(k)\right) - 2(1/k)^2 C(k) \tag{11}$$

$$L_h = 1 - 2i(1/k)C(k) \tag{12}$$

$$M_\alpha = (3/8) - i(1/k) \tag{13}$$

$$M_h = 0.5 \tag{14}$$

where $C(k)$ is Theodorsen's function [24],

$$C(k) = \frac{H_1^{(2)}(k)}{H_1^{(2)}(k) + iH_0^{(2)}(k)} \tag{15}$$

and $H_n^{(2)}$ are Hankel functions with $\nu = n$. (See [27] page 359). The reduced frequency is defined in terms of the frequency in radians ω, the wing chord and the free stream velocity U_∞ as

$$k = \frac{\omega b}{U_\infty}. \tag{16}$$

Acknowledgments

We would like to thank Phil Beran and Mohammed Kurdi for providing the model of the nonlinear, aeroelastic airfoil, and Frank Eastep for his help in developing the Goland wing model and his insight into that problem. This work was supported by the Air Force Office of Scientific Research under the AFOSR/ASEE Summer Faculty

Fellowship program, and performed in the Air Vehicles (RB) directorate of the Air Force Research Laboratory at Wright Pattern Air Force Base, under the direction of Dr. Jose Camberos.

References

[1] G. M. Rebeiz, *RF MEMS Theory, Design and Technology*: Wiley, 2003.
[2] N. Cressie, *Statistics of Spatial Data*. New York: John Wiley and Sons, 1991.
[3] R. Ghanem and J. Red-Horse, "Propagation of probabilistic uncertainty in complex physical systems using a stochastic finite element approach," Los Alamos, NM, USA, 1999, pp. 137-44.
[4] S. Hosder, R. W. Walters, and M. Balch, "Efficient sampling for non-intrusive polynomial chaos applications with multiple uncertain input variables," Waikiki, HI, United States, 2007, pp. 2946-2961.
[5] S. Hosder, R. W. Walters, and R. Perez, "A non-intrusive polynomial chaos method for uncertainty propagation in CFD simulations," Reno, NV, United States, 2006, pp. 10649-10667.
[6] D. R. Millman, P. I. King, R. C. Maple, P. S. Beran, and L. K. Chilton, "Estimating the probability of failure of a nonlinear aeroelastic system," *Journal of Aircraft*, vol. 43, pp. 504-516, 2006.
[7] M. S. Eldred, A. A. Giunta, L. P. Swiler, S. F. Wojtkiewicz Jr., W. E. Hart, J.-P. Watson, D. M. Gay, and S. L. Brown, "DAKOTA, A Multilevel Parallel Object-Oriented Framework for Design Optimization, Parameter Estimation, Uncertainty Quantification, and Sensitivity Analysis. Version 4.1 Users Manual.," Sandia National Laboratories, Albuquerque, NM Sandia Technical Report SAND2001-3796, 2008.
[8] R. V. Field Jr, "SAND2005-3223: A decision-theoretic method for surrogate model selection," Sandia National Laboratories, Albuquerque, NM June 2005 2005.
[9] A. A. Giunta, J. M. McFarland, L. P. Swiler, and M. S. Eldred, "The promise and peril of uncertainty quantification using response surface approximations," *Structure and Infrastructure Engineering*, vol. 2, pp. 175-89, 2006.
[10] M. D. McKay, R. J. Beckman, and W. J. Conover, "COMPARISON OF THREE METHODS FOR SELECTING VALUES OF INPUT VARIABLES IN THE ANALYSIS OF OUTPUT FROM A COMPUTER CODE," *Technometrics*, vol. 21, pp. 239-245, 1979.
[11] M. D. McKay, R. J. Beckman, and W. J. Conover, "Comparison of three methods for selecting values of input variables in the analysis of output from a computer code," *Technometrics*, vol. 42, pp. 55-61, 2000.
[12] J. Hammersley, "Monte Carlo methods for solving multivariable problems," *Proceedings of the New York Academy of Science*, vol. 86, pp. 844-874, 1960.
[13] L. Kocis and W. J. Whiten, "Computational investigations of low-discrepancy sequences," *ACM Transactions on Mathematical Software*, vol. 23, pp. 266-94, 1997.
[14] V. J. Romero, J. V. Burkardt, M. D. Gunzburger, and J. S. Peterson, "Comparison of pure and "Latinized" centroidal Voronoi tessellation against various other statistical sampling methods," *Reliability Engineering and System Safety*, vol. 91, pp. 1266-1280, 2006.
[15] M. Matsumoto and T. Nishimura, " Mersenne Twister: A 623-Dimensionally Equidistributed Uniform Pseudorandom Number Generator," *ACM Transactions on Modeling and Computer Simulation,*, vol. 8, pp. 3-30, 1998.
[16] H. O. Madsen, "First order vs. second order reliability analysis of series structures," *Structural Safety*, vol. 2, pp. 207-214, 1985.
[17] A. Basudhar and S. Missoum, "A Sampling-Based Approach for Probabilistic Design with Random Fields," in *49th AIAA/ASME/ASCE/AHS/ASC Structures, Structural Dynamics, and Materials Conference* Schaumburg, IL, 2008.
[18] S. Donders, J. Van de Peer, S. Dom, H. Van Der Auweraer, and D. Vandepitte, "Parameter Uncertainty and Variability in the Structural Dynamics Modeling Process," in *22nd International Modal Analysis Conference (IMAC XXII)*, Dearborne, Michigan, 2004.
[19] J. W. Wittwer, M. S. Baker, and L. L. Howell, "Robust design and model validation of nonlinear compliant micromechanisms," *Journal of Microelectromechanical Systems*, vol. 15, pp. 33-41, 2006.
[20] M. Allen, M. Raullin, K. Maute, and D. M. Frangopol, "Reliability-based analysis and design optimization of electrostatically actuated MEMS," *Computers and Structures*, vol. 82, pp. 1007-1020, 2004.
[21] A. Ang and W. Tang, *Probability Concepts in Engineering Planning and Design: Vol. 1 - Basic Principles*. New York, NY: John Wiley and Sons, Inc., 1975.
[22] B. H. K. Lee, Jiang, L.Y., and Y. S. Wongf, "FLUTTER OF AN AIRFOIL WITH A CUBIC NONLINEAR RESTORING FORCE," in *A98-25026, AIAA-98-1725*, 1998.

[23] S. Missoum, P. S. Beran, M. Kurdi, and D. M. McFarland, "Reliability-based design optimization of nonlinear aeroelastic problems," in *49th AIAA/ASME/ASCE/AHS/ASC Structures, Structural Dynamics, and Materials Conference* Schaumburg, IL, 2008.
[24] R. L. Bisplinghoff, H. Ashley, and R. L. Halfman, *Aeroelasticity*. New York: Dover, 1996.
[25] P. S. Beran, N. S. Khot, F. E. Eastep, R. D. Snyder, and J. V. Zweber, "Numerical analysis of store-induced limit-cycle oscillation," *Journal of Aircraft*, vol. 41, pp. 1315-1326, 2004.
[26] B. W. Silverman, *Density Estimation for Statistics and Data Analysis*. London: Chapman and Hall, 1986.
[27] M. Abramowitz and I. A. Stegun, *Handbook of Mathematical Functions*, 9th ed. New York: Dover, 1972.